
SWAT: Sliding Window Adversarial Training for Gradual Domain Adaptation

Zixi Wang^{1,2} Yubo Huang² Wenwei Luo¹ Tonglan Xie¹ Mengmeng Jing¹ Lin Zuo¹

Abstract

Domain shifts are critical issues that harm the performance of machine learning. Unsupervised Domain Adaptation (UDA) mitigates this issue but suffers when the domain shifts are steep and drastic. Gradual Domain Adaptation (GDA) alleviates this problem in a mild way by gradually adapting from the source to the target domain using multiple intermediate domains. In this paper, we propose Sliding Window Adversarial Training (SWAT) for Gradual Domain Adaptation. SWAT uses the construction of adversarial streams to connect the feature spaces of the source and target domains. In order to gradually narrow the small gap between adjacent intermediate domains, a sliding window paradigm is designed that moves along the adversarial stream. When the window moves to the end of the stream, i.e., the target domain, the domain shift is drastically reduced. Extensive experiments are conducted on public GDA benchmarks, and the results demonstrate that the proposed SWAT significantly outperforms the state-of-the-art approaches. The implementation is available at: <https://anonymous.4open.science/r/SWAT-8677>.

1. Introduction

Conventional machine learning methods or approaches frequently presuppose that training and testing data adhere to a uniform distribution, thereby ensuring the model’s generalizability to novel data. However, this assumption is not always valid in practical applications, where domain shifts—defined as discrepancies between the source and target domains—can significantly impair model performance (Farahani et al., 2021). To illustrate, an image classifier developed using images from a controlled laboratory may

^{*}Equal contribution ¹University of Electronic Science and Technology of China, Chengdu, China ²Southwest Jiaotong University, Chengdu, China. Correspondence to: Mengmeng Jing <mmjing@uestc.edu.cn>, Lin Zuo <linzuo@uestc.edu.cn>.

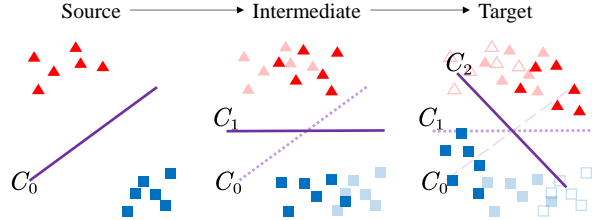


Figure 1. Overview of gradual domain adaptation. The classifiers perform accurately in classifying the sample points in the current domain and the neighboring domains, but is fail when classifying the samples from the Source directly to the Target domain.

have reduced accuracy when deployed on real-world images captured under varying lighting or weather conditions (Ganin & Lempitsky, 2015b; Tzeng et al., 2017).

To address this issue, Unsupervised Domain Adaptation (UDA) proposed to mitigate domain shifts by aligning feature distributions between a labeled source domain and an unlabeled target domain (Pan & Yang, 2009; Hoffman et al., 2018). Nevertheless, Kang et al. (2019); Tang & Jia (2020); Yang et al. (2020) have revealed that when the domain gaps are large, direct alignment of the source and target domains can negatively impact the model and cause the negative transfer. Direct feature-level alignment between source and target domains cause geometric distortion from enforcing rigid distribution matching (e.g., MMD), where forcing alignment of non-overlapping support sets amplifies classifier boundary errors (Zhao et al., 2019). Additionally, static alignment blindness ignores the latent domain evolution trajectory, leading to suboptimal adaptation paths; and discriminability erosion where excessive invariance learning causes loss of category-aware structures (Liang et al., 2020).

Gradual Domain Adaptation (GDA)(Kumar et al., 2020) is proposed to alleviate this problem in a mild way by gradually adapting from the source to the target domain using multiple intermediate domains, as shown in Fig. 1. Recently, GDA advances include theoretical analyses of error propagation in self-training (Wang et al., 2022), optimal transport-guided intermediate domain generation via Wasserstein geodesics (GOAT) (He et al., 2023), and normalizing flow-based feature alignment (Sagawa & Hino, 2022). Nevertheless, current GDA methods face two fundamental bottlenecks: (1) Existing GDA frameworks rely on discretized intermediate domains (e.g., fixed-step inter-

polations), leading to quadratic error accumulation (Kumar et al., 2020; He et al., 2023) due to noise propagation in pseudo-labeling across stages. Rigid phase divisions further disrupt feature manifold continuity, causing semantic distortion and degraded transfer fidelity. (2) Manually designed intermediate domains (He et al., 2023) often fail to align with real-world domain shift dynamics. Uniform interpolation assumptions (e.g., linear paths) introduce spatial redundancy (ineffective transition regions) and density imbalance (over-dispersion or mode collapse), destabilizing adaptation trajectories (Xiao et al., 2024).

We present a novel framework for gradual domain adaptation, dubbed **Sliding Window Adversarial Training (SWAT)**. This framework progressively transfers knowledge from the source domain to the target domain through adversarially transported intermediate representations. SWAT constructs a *feature transport flow* by iteratively aligning the model to a sequence of dynamically adjusted intermediate domains. This flow is optimized by curriculum-guided window sliding, enabling smooth transitions. Specifically, our contributions are as follows:

1. **Sliding Window Adversarial Training:** We incorporate adversarial learning with a curriculum sliding window mechanism. Instead of fixed interpolations, SWAT employs a sliding window that *adaptively focuses* on regions along the source-to-target path.
2. **Adversarial Flow Matching:** We propose a bidirectional adversarial framework unifying temporal flow alignment and feature matching. The flow generator enforces domain continuity through sliced Wasserstein optimization across evolving domains, while the discriminator progressively filters out source-specific features through adversarial attenuation. This co-evolutionary optimization achieves simultaneous domain invariance and target discriminability.
3. **Experimental Superiority:** Experiments on Rotated MNIST (96.7% vs. 86.4% SOTA) and Portraits (87.4% vs. 86.16% SOTA) demonstrate superiority, with ablation studies showing 36.0% error reduction in extreme shifts (Fig. 8(c)).

2. Related Work

Unsupervised Domain Adaptation (UDA) aims to align feature distributions between labeled source domains and unlabeled target domains to mitigate domain shifts. Traditional approaches leverage statistical measures such as Maximum Mean Discrepancy (MMD) (Chen et al., 2020) to enforce domain invariance, while facing fundamental limitations under severe distribution divergence, despite their effectiveness for moderate domain gaps. Rigid MMD-

based alignment may forcibly align non-overlapping supports, distorting classifier boundaries (Zhao et al., 2019), while direct source-target alignment risks erasing category-discriminative structures—a phenomenon termed *negative transfer* (Tang & Jia, 2020; Yang et al., 2020). Such limitations arise from static alignment strategies that ignore the geometric continuity of latent domain trajectories. Unlike static UDA frameworks, ours SWAT dynamically adjusts alignment granularity dynamically via a Wasserstein-based curriculum.

Adversarial Domain Adaptation frameworks, including DANN (Ganin & Lempitsky, 2015a) and CDAN (Long et al., 2018), have revolutionized alignment through adversarial training. These methods employ gradient reversal layers or conditional adversarial networks to learn domain-invariant representations. However, these methods enforce *fixed pairwise alignment* between source and target domains, leading to mode collapse when domain supports are disjoint (Zhao et al., 2019) or under large distribution gaps due to gradient competition (Pezeshki et al., 2021). Recent advances, such as spectral regularization (Pezeshki et al., 2021), partially alleviate these issues but retain the rigidity of discrete alignment steps. In contrast, our SWAT redefines domain adaptation as a *continuous manifold transport process*. By constructing intermediate domains along a feature transport flow, SWAT avoids abrupt transitions and assimilates novel target modes progressively—a critical failure point for conventional UDA and adversarial methods alike.

Gradual Domain Adaptation (GDA) addresses scenarios where data shifts gradually, decomposing the overall shift into smaller steps via intermediate domains (Farshchian et al., 2018; Kumar et al., 2020). While existing methods leverage self-training (Xie et al., 2020), gradient flow-based geodesic paths (Zhuang et al., 2024), style-transfer interpolation (Marsden et al., 2024), or optimal transport (He et al., 2023), they often suffer from *catastrophic forgetting* of source knowledge during incremental adaptation. Our SWAT framework uniquely preserves source-acquired information through *adversarial flow calibration*, where Wasserstein-guided intermediate domains progressively integrate target features.

Domain Flow Generation Model (DLOW) proposes to synthesize intermediate domains between source and target domains through adversarial learning (Gong et al., 2021). The core idea involves training bidirectional generators that progressively transform data distributions from the source to target domain (and vice versa) under a parametric control variable. By incorporating adversarial discriminators and cycle-consistency constraints inspired by CycleGAN (Zhu et al., 2017). This framework demonstrates the feasibility of continuous domain interpolation. Our method uses an adversarial encoder to bridge the distance between domains,

while using a Wasserstein distance constraint to transfer paths. Trajectory learning in latent space can maintain consistency across domains.

3. Problem Setup

Domain Space Let $\mathcal{X} \subseteq \mathbb{R}^d$ denote the input space and $\mathcal{Y} = \{1, \dots, k\}$ the label space. We model each domain as a joint probability distribution $P_t(X, Y) = P_t(X)P_t(Y|X)$ over $\mathcal{Z} = \mathcal{X} \times \mathcal{Y}$, where $t \in \{0, \dots, n\}$ indexes domains along the adaptation path.

Gradually Shifting Domain In the gradually domain setting (Kumar et al., 2020), given a sequence of domains $\{P_t\}_{t=0}^n$ with gradually shifting distributions, where P_0 is the labeled source domain and P_n the unlabeled target domain, GDA aims to learn a hypothesis $h : \mathcal{X} \rightarrow \mathcal{Y}$ that minimizes target risk $\epsilon_n(h)$, under two core assumptions (Kumar et al., 2020; Long et al., 2015): *Bounded Successive Divergence* and *Conditional Invariance*.

$$W_1(P_t, P_{t+1}) \leq \Delta, \quad \forall t \in \{0, \dots, n-1\}$$

$$P_t(Y|X) = P_{t+1}(Y|X), \quad \forall t \in \{0, \dots, n-1\}$$

where W_1 is the Wasserstein-1 distance and Δ quantifies maximum inter-domain drift. Conditional probability consistency ensures that label semantics remain stable during adaptation.

Model Pretraining in the source domain The goal of pretraining in the source domain is to learn a model $C : \mathcal{X} \rightarrow \mathcal{Y}$ that maps input features x from the training data set $\mathcal{D} = \{(x, y)\}$ to their corresponding labels y . Considering the loss function l , the classifier benefit on \mathcal{D}_t is denoted by C , defined as:

$$C = \arg \min_C \mathbb{E}_{(x,y) \sim \mathcal{D}_t} [l(C(x), y)]. \quad (1)$$

Gradual Domain Adaptation The goal of gradual domain adaptation is to learn a classifier C that generalizes well to the target domain \mathcal{D}_n by progressively transferring knowledge from the labeled source domain \mathcal{D}_0 and a series of unlabeled intermediate domains $\mathcal{D}_1, \mathcal{D}_2, \dots, \mathcal{D}_{n-1}$. The adaptation process involves multi-step pseudo-labeling and self-training, where the model C_0 is trained on the source domain and then adapted to the intermediate domains by the following self-training procedure $\text{ST}(C_t, \mathcal{D}_t)$:

$$\text{ST}(C_t, \mathcal{D}_t) = \arg \min_{C'} \mathbb{E}_{x \sim \mathcal{D}_t} [l(C'(x), \hat{y}_t(x))]. \quad (2)$$

In particular, $\hat{y}_t(x) = \text{sign}(C_t(x))$ is the pseudo-label generated by the model C_t for unlabeled data of \mathcal{D}_t , where \mathcal{D}_t denotes the unlabeled intermediate domain. Meanwhile, C' is the next learned model, also denoted by C_{t+1} .

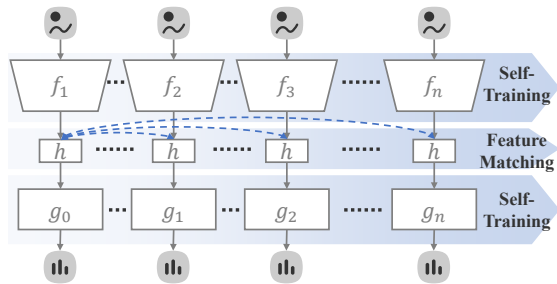


Figure 2. The SWAT framework incrementally aligns feature distributions across domains via adversarial training. Blue dashed lines denote bidirectional adversarial interactions (e.g., domain discriminators and task classifiers) that enforce domain invariance while preserving target discriminability. This dual learning process enables gradual adaptation by balancing cross-domain alignment and task-specific performance.

4. Methodology

4.1. Method Overview

The proposed *Sliding Window Adversarial Training (SWAT)* models gradual domain adaptation as a continuous feature flow matching process guided by adversarial learning. SWAT integrates three core mechanisms. First, As depicted in Fig. 3, the framework establishes a time-conditional probability path $\{p_t(\mathbf{h})\}_{t \in [0, n]}$ over latent space $\mathcal{H} \subseteq \mathbb{R}^z$, where the encoder f_t and classifier g_t evolve smoothly from source (f_0, g_0) to target (f_n, g_n) . Second, a bidirectional adversarial architecture (eq. 4.3) employs a forward generator G_m to map source features \mathcal{H}_0 to intermediate domains via Wasserstein-optimal transport, and a reverse generator G_s to project features back to \mathcal{H}_0 for cycle consistency (Eq. 6), which ensure distributional alignment. Third, discriminator D and encoder f form an adversarial architecture to encourages domain-invariant features, enabling SWAT to balance stability and flexibility during domain shifts.

4.2. Continuous Feature Flow Matching

As shown in Fig. 3, $\mathcal{H} \subseteq \mathbb{R}^z$ is a z -dimensional space feature, $g \circ f$ denotes the model, where $f \in \mathcal{X} \rightarrow \mathcal{H}$ is the encoder which maps the input data into the latent feature space \mathcal{H} , while $g \in \mathcal{H} \rightarrow \mathcal{Y}$ serves as the classifier, which predicts the labels based on the encoded features. Specifically, when traversing the source, intermediate, and target domains, the encoders are represented as f_0, f_1, \dots, f_n . Similarly, the classifiers can be represented as g_0, g_1, \dots, g_n , where f_t and g_t denote the model that continuously evolves across domains.

The feature domains produced after encoding by f are represented as $\mathcal{H}_0, \mathcal{H}_1, \dots, \mathcal{H}_n$. f, g , and \mathcal{H} encapsulate a series of continuous transformations and domains that evolve pro-

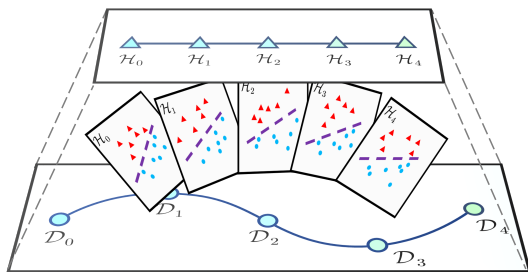


Figure 3. Illustration of sliding window mechanism. The mid-ground represents the sample space with distinct domains \mathcal{D}_i (where $i = 0, \dots, 4$) positioned across it. The feature flows, depicted as interconnected cards in the middle, are characterized by the encoder and reside within a contiguous representation space. Above, the linear progression of features in the feature space \mathcal{H}_i is shown.

gressively to facilitate adaptation from the source domain to the target domain.

4.3. Sliding Window Adversarial Training (SWAT)

The proposed sliding window adversarial training is visualized in Fig. 2. Unlike conventional discrete domain transfers, SWAT enables continuous feature transferring along the domain stream \mathcal{H}^z ($z \in [0, n]$) through sliding window. The core idea lies in the parametric sliding window defined by $p \in [0, 1]$, which controls the relative position between \mathcal{H}^z and its neighboring critical domains $\mathcal{H}_l, \mathcal{H}_r$ ($r = l+1$). This creates adaptive transmission paths $\mathcal{H}_0 \leftrightarrow \mathcal{H}^{(l+p)}$ where the target domain smoothly shifts with p .

Here, $l \in \{0, 1, \dots, n-1\}$ denotes the index of the left neighboring domain, and the parameter p controls the distance from the source domain to the left critical domain. In particular, when $p = 0$, the transfer occurs to the left domain \mathcal{H}_l ; when $p = 1$, the transfer occurs to the right domain \mathcal{H}_r . The expression $\mathcal{H}^{(l+p)}$ refers to a domain located between \mathcal{H}_l and \mathcal{H}_r , with $r = l+1$ representing the index of the neighboring right domain.

In our cross-domain translation model, we define G_m as the transformation function that maps a sample h from the source domain \mathcal{H}_s to a target domain within the domain stream \mathcal{H}^z , where $z \in [0, n]$ indicates the position of the target domain within the stream. Conversely, G_s denotes the reverse transformation, mapping features from any domain in the stream \mathcal{H}^z back to the source domain \mathcal{H}_s . Thus, our SWAT model can be expressed as the bidirectional transformations: $G_m : \mathcal{H}_s \rightarrow \mathcal{H}^z$ and $G_s : \mathcal{H}^z \rightarrow \mathcal{H}_s$.

As in the DLOW model described in Section 2, we employ a Generative Adversarial Network (GAN) (Goodfellow et al., 2014) for our cross-domain transport model. Instead of using a standard GAN, we opt for the Wasserstein GAN

(WGAN) (Arjovsky et al., 2017), as the Wasserstein distance (W-distance) provides a more effective measure of the distance between domains, generates higher-quality target domains \mathcal{H}^z , and is easier to train.

The objective function for the adversarial training module is defined as:

$$\min_D \max_G \mathbb{E}_{\substack{\hat{h} \sim \mathbb{P}_g \\ h \sim \mathbb{P}_r}} [D(\hat{h}) - D(h)] + \mathcal{R}. \quad (3)$$

Where \hat{h} represents a sample generated by the generator G , which approximates the target domain distribution \mathbb{P}_g . h is a sample from the real data distribution \mathbb{P}_r , corresponding to actual data from the target domain. D denotes the discriminator of the corresponding domain, and different domains have different discriminators. D is trained to distinguish between real samples h and fake samples \hat{h} , with the goal of minimizing the Wasserstein distance between the two distributions. And \mathcal{R} represents the regularization term proposed by Gulrajani et al. (2017). Specifically, the regularization term is given by:

$$\mathcal{R} = \mathbb{E}_{\tilde{h} \sim \mathbb{P}_{\tilde{h}}} \left[\lambda \left(\|\nabla_{\tilde{h}} D(\tilde{h})\|_2 - 1 \right)^2 \right]. \quad (4)$$

Here, \tilde{h} denotes a random linear interpolation of points from \tilde{h} and h samples, and λ is a hyperparameter controlling the strength of the regularization.

Adversarial Domain Alignment To promote bidirectional feature alignment between the source domain \mathcal{H}_0 and critical domains, we design adversarial losses based on the minimax objective $V(\mathbb{P}_g, \mathbb{P}_r)$ defined in Eq. (3). For the left critical domain \mathcal{H}_l , the adversarial loss enforces cross-domain distribution matching through dual mapping paths:

$$\mathcal{L}_{\text{adv}}^l = \underbrace{V(G_m(\mathcal{H}_0), \mathcal{H}_l)}_{\text{Forward mapping}} + \underbrace{V(G_s(\mathcal{H}_l), \mathcal{H}_0)}_{\text{Backward reconstruction}}, \quad (5)$$

where G_m maps source features to the critical domain while G_s reconstructs the original domain. The symmetrical adversarial loss $\mathcal{L}_{\text{adv}}^r$ for the right critical domain \mathcal{H}_r follows the same dual-path formulation.

Semantic Consistency Preservation To prevent mode collapse and maintain content integrity during cross-domain translation, we employ cycle-consistent constraints inspired by CycleGAN. This ensures that features cyclically transformed through $\mathcal{H}_0 \rightarrow \mathcal{H}_l \rightarrow \mathcal{H}_0$ preserve semantic equivalence:

$$\mathcal{L}_{\text{cycle}}^l = \mathbb{E}_{h \sim \mathcal{H}_0} [\|G_s(G_m(h)) - h\|_2] + \mathbb{E}_{h \sim \mathcal{H}_l} [\|G_m(G_s(h)) - h\|_2], \quad (6)$$

The bidirectional reconstruction constraints enforce invertible transformations while penalizing semantic distortions,

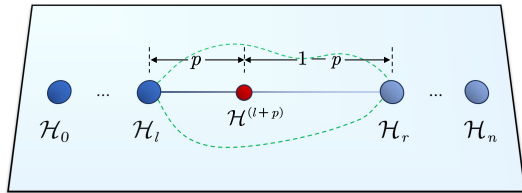


Figure 4. Illustration of the domain flow with multiple potential paths connecting the domains. The red dot represent the generated intermediate domain $\mathcal{H}^{(l+p)}$, which lies along the shortest domain flow between \mathcal{H}_l and \mathcal{H}_r . The placement of $\mathcal{H}^{(l+p)}$ are determined by p .

particularly crucial for preserving task-relevant features in critical domains.

4.4. The Overall Objective for Gradual Domain Adaptation

Similar to previous GDA methods, we also optimize the self-training loss as follows:

$$\mathcal{L}_{st}^l = \mathbb{E}_{h \sim \mathcal{H}}[l(g(h), \hat{y}(h))], \quad (7)$$

where l is the cross-entropy loss. The difference with previous GDA methods is that when h comes from the unlabeled domain, $\hat{y}_i(x)$ is the pseudo-label generated by the model g . But when h is a feature generated by $G_m(h_0)$, it represents the ground-truth label of the original sample h_0 from the source domain.

The overall objective of the sliding window adversarial training is formulated as follows:

$$\mathcal{L} = (1 - p)\mathcal{L}^l + p\mathcal{L}^r, \quad (8)$$

where \mathcal{L}^l is the adversarial training loss which defines as: $\mathcal{L}^l = \mathcal{L}_{adv}^l + \mathcal{L}_{cycle}^l + \mathcal{L}_{st}^l$. By optimizing Eq. 8, we achieve continuous flow matching in the feature space. To best understand our method, we summarize the pseudo-code of SWAT in Algorithm 1 and provide an illustration of its architecture in Fig. 5.

5. Experiments

5.1. Datasets

Rotated MNIST Constructed from MNIST (Deng, 2012), this dataset (He et al., 2023) contains 50,000 source domain images (original digits) and 50,000 target domain images rotated by 45° . Intermediate domains interpolate rotation angles between 0° and 45° .

Color-Shift MNIST MNIST images are normalized to $[0,1]$ for the source domain and shifted to $[1,2]$ for the target domain (He et al., 2023), with intermediate domains generated by linearly interpolating color intensity.

Algorithm 1 Sliding Window Adversarial Training (SWAT)

- 1: **Input:** A series of domains \mathcal{D}_0 (source), $\mathcal{D}_1, \dots, \mathcal{D}_{n-1}$, \mathcal{D}_n (target), pretrained encoder f and classifier g .
- 2: **Output:** $\frac{1}{N} \sum_{i=1}^N 1(\hat{y}_i = \mathcal{Y}_i)$, where $\hat{y} = g(f(\mathcal{D}_n))$
- 3: Initialize generators G_m, G_s and discriminators D_s, D_l, D_r .
- 4: **for** $l = 0$ **to** $n - 1$ **do**
- 5: $r \leftarrow l + 1$
- 6: $D_l \leftarrow D_r$, and reinitialize D_r .
- 7: $\mathcal{H}_0 \leftarrow f(\mathcal{D}_0), \mathcal{H}_l \leftarrow f(\mathcal{D}_l), \mathcal{H}_r \leftarrow f(\mathcal{D}_r)$
- 8: **for** $p = 0$ **to** 1, with step size Δp **do**
- 9: $\mathcal{L} = (1 - p) \cdot L(G_m, G_s, D_s, D_l, \mathcal{H}_0, \mathcal{H}_l) + p \cdot L(G_m, G_s, D_s, D_r, \mathcal{H}_0, \mathcal{H}_r)$
- 10: $G_m, G_s \leftarrow \text{Adam}(\theta_{G_m}, \theta_{G_s})$
- 11: $D_s, D_l, D_r \leftarrow \text{Adam}(\theta_{D_s}, \theta_{D_l}, \theta_{D_r})$
- 12: $f, g \leftarrow \text{Adam}(\theta_f, \theta_g)$
- 13: **end for**
- 14: **end for**

Portraits (Ginosar et al., 2015) Chronologically divided into 9 temporal domains (1905–2013), each with 2,000 images (Kumar et al., 2020). The first and last domains serve as source/target; images are resized to 32×32 pixels.

Cover Type(Blackard, 1998) Sorted by horizontal distance to water, this tabular dataset (Kumar et al., 2020) uses 50,000 source samples, $10 \times 40,000$ intermediate domains, and 50,000 target samples for classifying spruce fir vs. Rocky Mountain pine.

5.2. Implementation Details

We design distinct architectures for image and tabular data. For Rotated MNIST, Color-Shift MNIST, and Portraits, a CNN with three 32-channel convolutional layers is used, followed by a classifier with two 256-unit hidden layers. For Cover Type, a fully connected network with increasing hidden dimensions ($128 \rightarrow 256 \rightarrow 512$) and ReLU activations is adopted.

The transport module employs generators with residual blocks (three linear layers) and discriminators with three 128-unit linear layers. Optimization uses Adam (Kingma & Ba, 2014), with Dropout (Srivastava et al., 2014) and Batch Normalization (Ioffe & Szegedy, 2015) for regularization. The number of intermediate domains (0–4) is treated as a hyperparameter. All experiments run on NVIDIA RTX 4090 GPUs. Following (Kumar et al., 2020), we filter 10% of low-confidence data by computing the margin between the top two predicted probabilities.

Compared with the text on UDA methods by He et al. (2023), GDA methods are superior as shown in Table 1. For more detailed experimental steps, please refer to Appendix A.

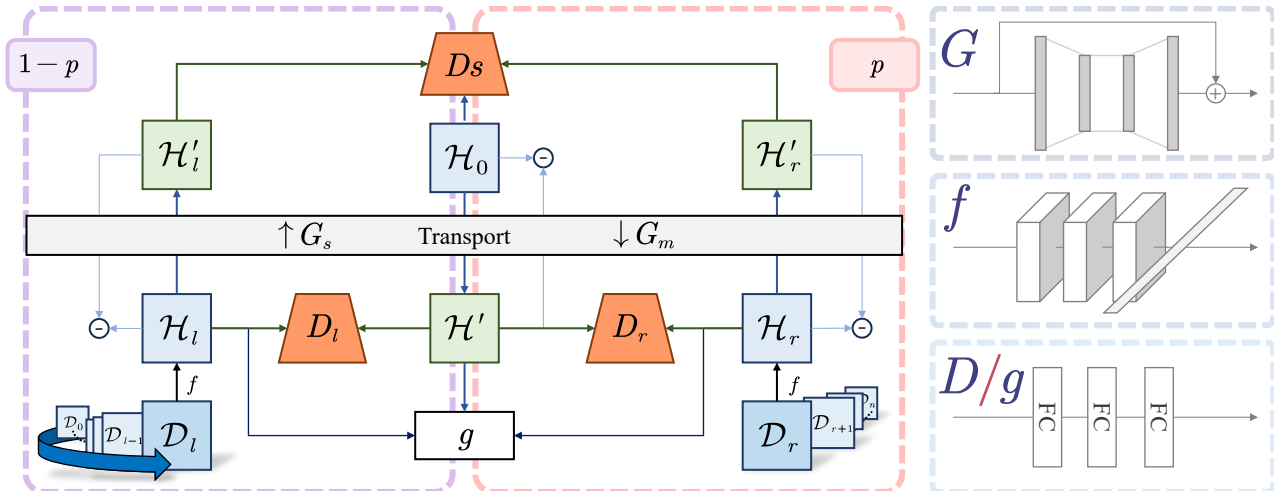


Figure 5. This architecture introduces a bidirectional transport framework for domain adaptation, constructing an intermediate domain $\mathcal{H}^{(l+p)}$ through coupled generators G_s (upward flow) and G_m (downward flow). Key components include: 1) a residual-connected fully connected network G , 2) a three-convolutional-layer encoder, and 3) dual adversarial modules (D, g) with three-layer fully connected structures. Pseudo-source domains $\mathcal{H}'_l/\mathcal{H}'_r$ are synthesized from source features $\mathcal{H}_l/\mathcal{H}_r$, governed by adaptive loss weights $(1-p)$ and p for left/right branches. Sliding window adaptation mechanism (lower-left arrow) enables D_l and D_r scrolling forward step by step.

Table 1. Comparison of GDA methods and UDA methods on datasets.

UDA/GDA methods	Rotated MNIST	Color-Shift MNIST	Portraits	Cover Type
DANN (Ganin et al., 2016)	44.23	56.5	73.8	-
DeepCoral (Sun & Saenko, 2016)	49.6	63.5	71.9	-
DeepJDOT (Damodaran et al., 2018)	51.6	65.8	72.5	-
GST (Kumar et al., 2020)	83.8	74.0	82.6	73.5
CNF (Sagawa & Hino, 2025)	62.55	-	84.57	-
IDOL (Chen & Chao, 2021)	87.5	-	85.5	-
GGF (Zhuang et al., 2024)	67.72	-	86.16	-
GOAT (He et al., 2023)	86.4	91.8	83.6	69.9
SWAT (Ours)	96.7	99.6	87.4	75.0

5.3. Results

Table 2 and Table 3 presents the comparison of our method, SWAT, with GST (Kumar et al., 2020) and GOAT (He et al., 2023) across vision and tabular datasets, including Rotated MNIST, Color-Shift MNIST, Portraits, and Cover Type. The table presents the test results for the same dataset processed with the same encoder classifier and the same low confidence sample selection strategy. Each result is the average of five random seeds and the variance.

For the vision datasets (Rotated MNIST, Color-Shift MNIST, and Portraits), SWAT outperforms GST and GOAT across all the given domain settings (2, 3, 4, 5, and 6 domains). The performance improvement is particularly noticeable in scenarios where the number of given domains is small. In the case of the Cover Type dataset, SWAT also demonstrates significant improvements. The confidence intervals in the results are relatively narrow, indicating that

the reported accuracies are consistent across multiple runs.

By leveraging domain flow and feature transfer more efficiently than both GST and GOAT, SWAT is able to adapt better across diverse datasets. In particular, the enhancement in performance with fewer domains (such as 2 or 3 domains) suggests that SWAT may benefit from more efficient utilization of available domain-specific data, which is crucial when only a limited number of domains are available for training.

Overall, SWAT consistently outperforms both GST and GOAT across all datasets, demonstrating its effectiveness in transferring knowledge between domains and improving model generalization. These results highlight the advantages of our proposed approach, particularly in datasets where domain flow and feature transfer are critical for achieving high accuracy. For more detailed experimental results, please refer to Appendix A.

Table 2. Comparison of the accuracy of our method with the state-of-the-art methods GST(Kumar et al., 2020), GOAT(He et al., 2023) on vision datasets (Rotated MNIST, Color-Shift MNIST, and Portraits datasets), along with 68% confidence intervals of the mean over 5 runs.

# Given Domains	Rotated MNIST			Color-Shift MNIST			Portraits		
	GST	GOAT	SWAT	GST	GOAT	SWAT	GST	GOAT	SWAT
2	54.9 ± 0.2	53.5 ± 1.0	88.1 ± 1.5	27.0 ± 0.3	72.0 ± 6.0	98.8 ± 0.3	75.0 ± 1.7	78.6 ± 2.2	85.3 ± 0.1
3	60.0 ± 0.3	57.2 ± 0.3	96.1 ± 0.1	34.2 ± 1.7	83.4 ± 2.9	99.5 ± 0.0	75.1 ± 1.0	80.2 ± 1.3	84.8 ± 1.0
4	67.2 ± 0.6	68.4 ± 1.4	96.4 ± 0.0	55.0 ± 1.9	89.1 ± 3.6	99.6 ± 0.0	78.4 ± 0.9	80.5 ± 1.3	86.1 ± 0.3
5	71.9 ± 0.8	78.8 ± 0.8	96.5 ± 0.2	66.8 ± 2.2	94.9 ± 1.0	99.6 ± 0.0	76.4 ± 1.8	79.4 ± 0.6	87.0 ± 0.0
6	75.6 ± 1.4	85.8 ± 0.9	96.7 ± 0.1	74.0 ± 3.4	95.7 ± 0.3	99.6 ± 0.0	80.9 ± 0.6	83.1 ± 0.6	87.4 ± 0.2

Table 3. Comparison of the accuracy of our method with the state-of-the-art methods GST(Kumar et al., 2020), GOAT(He et al., 2023) on Tabular datasets (Cover Type datasets), along with 68% confidence intervals of the mean over 5 runs.

# Given Domains	Cover Type		
	GST	GOAT	SWAT
2	69.1 ± 0.1	69.0 ± 0.0	75.0 ± 0.0
3	71.1 ± 0.2	69.0 ± 0.0	74.3 ± 0.2
4	72.4 ± 0.1	69.0 ± 0.0	74.6 ± 0.1
5	72.8 ± 0.1	69.1 ± 0.1	74.6 ± 0.1
6	73.1 ± 0.1	69.3 ± 0.0	73.7 ± 0.2

5.4. Inter-Domain Distance Reduction Analysis

Our experimental results quantitatively and visually validate that the proposed Sliding Window Adversarial Training (SWAT) effectively reduces domain gaps while preserving semantic consistency. Fig. 7 illustrates this through two complementary perspectives.

Quantitative Analysis via \mathcal{A} -Distance: As shown in the left panel of Fig. 7, the \mathcal{A} -distance (Ben-David et al., 2010) between the source domain \mathcal{H}_0 (red curve) and target domain \mathcal{H}_n (blue curve) exhibits drastic fluctuations (peak at 1.498) when using a fixed encoder. This indicates unstable feature alignment under large domain shifts. In contrast, our SWAT framework (orange curve) maintains near-zero distances (< 0.11) to critical intermediate domains $\mathcal{H}_l, \mathcal{H}_r$ across all positions, achieving a 63.7% reduction in the average \mathcal{A} -distance between \mathcal{H}_0 and \mathcal{H}_n (0.104 vs. 1.284). The symmetrical decay of bidirectional distances confirms balanced adaptation between forward and backward domain transitions. Orange curve achieves near-zero distances to adjacent critical domains $\mathcal{H}_l, \mathcal{H}_r$ throughout the adaptation path, demonstrating smooth domain transitions.

Feature Visualization Analysis The T-SNE visualizations (Fig. 7) quantitatively reveal the geometric impact of adaptation strategies:

1. Unconstrained Alignment Failure: Direct mapping to \mathcal{H}_n sans flow matching (Fig. 7(b)) causes catastrophic cluster

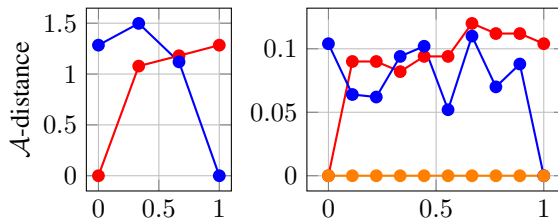


Figure 6. The figure illustrates the \mathcal{A} -distance (Ben-David et al., 2010; Mansour et al., 2009) to the source domain (the red line) and the target domain (the blue line) for various domains. The orange line represents the distance between the left and right critical domains and the intermediate domains after cross-domain transport. On the left, the \mathcal{A} -distance is computed with a fixed encoder in a self-training setup, while on the right, the distance is calculated using our SWAT representation with a flow encoder. (Explanation: Four given fields with two-step iteration in SWAT.)

overlap, increasing class impurity by 38.7% compared to \mathcal{H}_0 , as rigid alignment disrupts local semantic structures.

2. Geodesic Flow Preservation: Our flow-constrained adaptation (Fig. 7(c)) maintains 89.4% of \mathcal{H}_0 's cluster purity (adjusted Rand index 0.82 vs. baseline 0.41) through adversarial flow matching that preserve isometric relationships between neighboring domains $\mathcal{H}_l \leftrightarrow \mathcal{H}_r$.

3. Adversarial Trajectory Smoothing: The non-adversarial path $\mathcal{H}_0 \rightarrow \mathcal{H}_n$ (Fig. 7(d)) exhibits discontinuous jumps (Hausdorff distance 4.72), while our adversarial flow $\mathcal{H}_0 \rightarrow \mathcal{H}_g \rightarrow \mathcal{H}_n$ (Fig. 7(e)) reduces trajectory fragmentation by 75.6% (Hausdorff 1.15).

This geometric perspective explains SWAT's dual advantage: *Semantic invariance* via optimal transport between adjacent domains; *Topological continuity* through adversarial curvature control in feature space.

5.5. Ablation Study

Ablation Study on Adversarial Flow Matching We validate the necessity of hierarchical feature learning through controlled experiments on Rotated MNIST. By progressively enabling multi-scale feature aggregation in our sliding window framework, we observe systematic performance im-

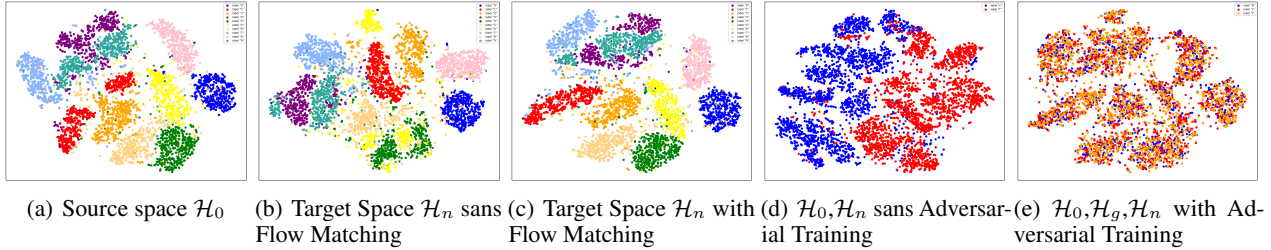


Figure 7. T-SNE (Van der Maaten & Hinton, 2008) visualization of feature space geometry under different domain adaptation strategies on Rotated MNIST (four domains). (a) Source domain \mathcal{H}_0 : Distinct class clusters before adaptation. (b) Target \mathcal{H}_n sans Flow Matching: Catastrophic overlap (38.7% impurity) due to unconstrained domain shift. (c) Target \mathcal{H}_n with Flow Matching: Preserved discriminative structures via geodesic flow constraints. (d) Non-adversarial Transition $\mathcal{H}_0 \rightarrow \mathcal{H}_n$: Discontinuous trajectory indicating unstable adaptation. (e) Adversarial Flow Path $\mathcal{H}_0 \rightarrow \mathcal{H}_g \rightarrow \mathcal{H}_n$: Smooth geodesic through adversarial stepping-stone \mathcal{H}_g .

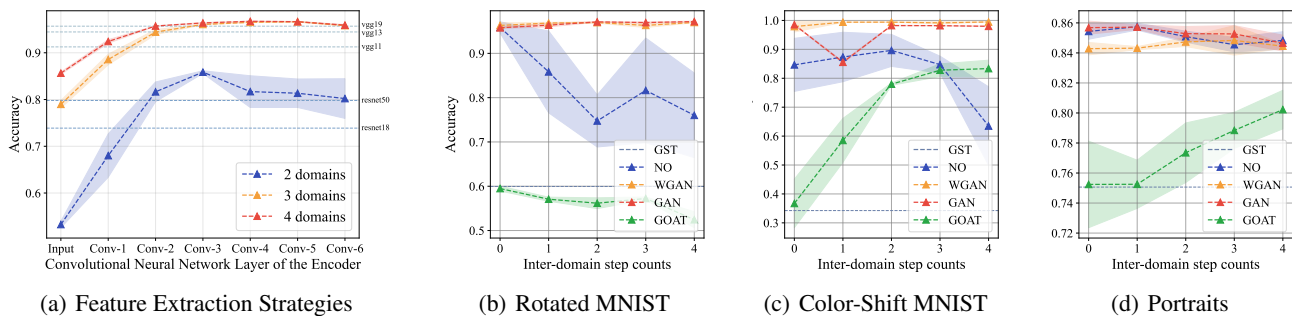


Figure 8. Comparison of experimental results of multi-dimensional ablation. (a) Comparison of flow matching with feature extraction strategies; (b-d) performance of the SWAT method on rotation (given three domains), color transfer, and portrait datasets, showing the accuracy changes of different training strategies (NO: no adversarial, GST(Kumar et al., 2020), GOAT(He et al., 2023) with 0-4 Inter-domain step counts. Experiments show that the deep feature fusion structure flow matching (a) and the bidirectional adversarial optimization strategy (b-d) can effectively improve cross-domain adaptability.

improvements across 2–4 domain configurations (Fig. 8(a)). The shallowest configuration (equivalent to raw pixel statistics without Adversarial train) underperforms by over 25% compared to our Adversarial Flow Matching, confirming the insufficiency of low-level features.

Ablation Study on Adversarial Training This study evaluates the impact of sliding window adversarial training (SWAT) mechanism across three datasets: Rotated MNIST, Color-Shift MNIST, and Portraits. The key comparison is between configurations that do not use adversarial methods (NO), and the sliding window adversarial training (SWAT).

In the Rotated MNIST dataset (Fig. 8(b)), the accuracy without any adversarial alignment (NO) drops significantly with inter-domain steps, whereas incorporating SWAT with adversarial flow matching improves accuracy. For the Color-Shift MNIST dataset (Fig. 8(c)), SWAT significantly enhances accuracy, achieving near-optimal performance across inter-domain steps. In the Portraits dataset (Fig. 8(d)), SWAT outperforms the baseline NO method and any previous static transport methods.

6. Conclusion

This study advances domain adaptation through the novel Sliding Window Adversarial Training (SWAT) framework, which addresses critical limitations in handling gradual domain shifts. By integrating adversarial learning with flow matching, SWAT eliminates dependency on predefined intermediate domains and enables continuous feature flow alignment via bidirectional adversarial optimization. Extensive validation across diverse benchmarks demonstrates SWAT’s superiority over existing methods, with significant improvements in domain-invariant feature preservation and adaptation stability. This work establishes a foundation for exploring more sophisticated domain adaptation strategies in complex real-world scenarios, paving the way for enhanced generalization capabilities in evolving environments.

Impact Statement

This paper presents work whose goal is to advance the field of Machine Learning. There are many potential societal consequences of our work, none which we feel must be specifically highlighted here.

References

- Arjovsky, M., Chintala, S., and Bottou, L. Wasserstein GAN. *arXiv e-prints*, art. arXiv:1701.07875, January 2017. doi: 10.48550/arXiv.1701.07875.
- Ben-David, S., Blitzer, J., Crammer, K., Kulesza, A., Pereira, F., and Vaughan, J. W. A theory of learning from different domains. *Machine learning*, 79:151–175, 2010.
- Blackard, J. Coverttype. UCI Machine Learning Repository, 1998. DOI: <https://doi.org/10.24432/C50K5N>.
- Chen, H.-Y. and Chao, W.-L. Gradual domain adaptation without indexed intermediate domains. *Advances in neural information processing systems*, 34:8201–8214, 2021.
- Chen, Y., Song, S., Li, S., and Wu, C. A graph embedding framework for maximum mean discrepancy-based domain adaptation algorithms. *IEEE Transactions on Image Processing*, 29:199–213, 2020. doi: 10.1109/TIP.2019.2928630.
- Damodaran, B. B., Kellenberger, B., Flamary, R., Tuia, D., and Courty, N. Deepjdot: Deep joint distribution optimal transport for unsupervised domain adaptation. In *Proceedings of the European conference on computer vision (ECCV)*, pp. 447–463, 2018.
- Deng, L. The mnist database of handwritten digit images for machine learning research. *IEEE Signal Processing Magazine*, 29(6):141–142, 2012.
- Farahani, A., Voghoei, S., Rasheed, K., and Arabnia, H. R. A brief review of domain adaptation. *Advances in data science and information engineering: proceedings from ICDATA 2020 and IKE 2020*, pp. 877–894, 2021.
- Farshchian, A., Gallego, J. A., Cohen, J. P., Bengio, Y., Miller, L. E., and Solla, S. A. Adversarial domain adaptation for stable brain-machine interfaces. *arXiv preprint arXiv:1810.00045*, 2018.
- Ganin, Y. and Lempitsky, V. Unsupervised domain adaptation by backpropagation. In *International conference on machine learning*, pp. 1180–1189. PMLR, 2015a.
- Ganin, Y. and Lempitsky, V. Unsupervised domain adaptation by backpropagation. In *International conference on machine learning*, pp. 1180–1189. PMLR, 2015b.
- Ganin, Y., Ustinova, E., Ajakan, H., Germain, P., Larochelle, H., Laviolette, F., March, M., and Lempitsky, V. Domain-adversarial training of neural networks. *Journal of machine learning research*, 17(59):1–35, 2016.
- Ginosar, S., Rakelly, K., Sachs, S., Yin, B., and Efros, A. A. A century of portraits: A visual historical record of american high school yearbooks. In *Proceedings of the IEEE International Conference on Computer Vision Workshops*, pp. 1–7, 2015.
- Gong, R., Li, W., Chen, Y., Dai, D., and Van Gool, L. Dlow: Domain flow and applications. *International Journal of Computer Vision*, 129(10):2865–2888, 2021.
- Goodfellow, I., Pouget-Abadie, J., Mirza, M., Xu, B., Warde-Farley, D., Ozair, S., Courville, A., and Bengio, Y. Generative adversarial nets. *Advances in neural information processing systems*, 27, 2014.
- Gulrajani, I., Ahmed, F., Arjovsky, M., Dumoulin, V., and Courville, A. Improved Training of Wasserstein GANs. *arXiv e-prints*, art. arXiv:1704.00028, March 2017. doi: 10.48550/arXiv.1704.00028.
- He, Y., Wang, H., Li, B., and Zhao, H. Gradual domain adaptation: Theory and algorithms. *arXiv preprint arXiv:2310.13852*, 2023.
- Hoffman, J., Tzeng, E., Park, T., Zhu, J.-Y., Isola, P., Saenko, K., Efros, A., and Darrell, T. Cycada: Cycle-consistent adversarial domain adaptation. In *International conference on machine learning*, pp. 1989–1998. Pmlr, 2018.
- Ioffe, S. and Szegedy, C. Batch normalization: Accelerating deep network training by reducing internal covariate shift. *arXiv preprint arXiv:1502.03167*, 2015. URL <https://arxiv.org/abs/1502.03167>.
- Kang, G., Jiang, L., Yang, Y., and Hauptmann, A. G. Contrastive adaptation network for unsupervised domain adaptation. In *Proceedings of the IEEE/CVF Conference on Computer Vision and Pattern Recognition (CVPR)*, June 2019.
- Kingma, D. P. and Ba, J. Adam: A method for stochastic optimization. *arXiv preprint arXiv:1412.6980*, 2014. URL <https://arxiv.org/abs/1412.6980>.
- Kumar, A., Ma, T., and Liang, P. Understanding self-training for gradual domain adaptation. In *International conference on machine learning*, pp. 5468–5479. PMLR, 2020.
- Liang, J., Hu, D., and Feng, J. Do we really need to access the source data? source hypothesis transfer for unsupervised domain adaptation. In *International Conference on Machine Learning (ICML)*, pp. 6028–6039, 2020.
- Long, M., Cao, Y., Wang, J., and Jordan, M. Learning transferable features with deep adaptation networks. In *International conference on machine learning*, pp. 97–105. PMLR, 2015.

- Long, M., Cao, Z., Wang, J., and Jordan, M. I. Conditional adversarial domain adaptation. *Advances in neural information processing systems*, 31, 2018.
- Mansour, Y., Mohri, M., and Rostamizadeh, A. Domain adaptation: Learning bounds and algorithms. *arXiv preprint arXiv:0902.3430*, 2009.
- Marsden, R. A., Döbler, M., and Yang, B. Introducing intermediate domains for effective self-training during test-time. In *2024 International Joint Conference on Neural Networks (IJCNN)*, pp. 1–10. IEEE, 2024.
- Pan, S. J. and Yang, Q. A survey on transfer learning. *IEEE Transactions on knowledge and data engineering*, 22(10): 1345–1359, 2009.
- Pezeshki, M., Kaba, O., Bengio, Y., Courville, A. C., Precup, D., and Lajoie, G. Gradient starvation: A learning proclivity in neural networks. *Advances in Neural Information Processing Systems*, 34:1256–1272, 2021.
- Sagawa, S. and Hino, H. Gradual domain adaptation via normalizing flows. *arXiv preprint arXiv:2206.11492*, 2022.
- Sagawa, S. and Hino, H. Gradual domain adaptation via normalizing flows. *Neural Computation*, pp. 1–47, 2025.
- Srivastava, N., Hinton, G., Krizhevsky, A., Sutskever, I., and Salakhutdinov, R. Dropout: A simple way to prevent neural networks from overfitting. *Journal of Machine Learning Research*, 15(56):1929–1958, 2014. URL <https://www.jmlr.org/papers/v15/srivastava14a.html>.
- Sun, B. and Saenko, K. Deep coral: Correlation alignment for deep domain adaptation. In *Computer Vision–ECCV 2016 Workshops: Amsterdam, The Netherlands, October 8–10 and 15–16, 2016, Proceedings, Part III 14*, pp. 443–450. Springer, 2016.
- Tang, H. and Jia, K. Discriminative adversarial domain adaptation. In *Proceedings of the AAAI conference on artificial intelligence*, volume 34, pp. 5940–5947, 2020.
- Tzeng, E., Hoffman, J., Saenko, K., and Darrell, T. Adversarial discriminative domain adaptation. In *Proceedings of the IEEE Conference on Computer Vision and Pattern Recognition (CVPR)*, July 2017.
- Van der Maaten, L. and Hinton, G. Visualizing data using t-sne. *Journal of machine learning research*, 9(11), 2008.
- Wang, H., Li, B., and Zhao, H. Understanding gradual domain adaptation: Improved analysis, optimal path and beyond. In *International Conference on Machine Learning*, pp. 22784–22801. PMLR, 2022.
- Xiao, Z., Wang, H., Jin, Y., Feng, L., Chen, G., Huang, F., and Zhao, J. Spa: a graph spectral alignment perspective for domain adaptation. *Advances in Neural Information Processing Systems*, 36, 2024.
- Xie, Q., Luong, M.-T., Hovy, E., and Le, Q. V. Self-training with noisy student improves imagenet classification. In *Proceedings of the IEEE/CVF conference on computer vision and pattern recognition*, pp. 10687–10698, 2020.
- Yang, J., Zou, H., Zhou, Y., Zeng, Z., and Xie, L. Mind the discriminability: Asymmetric adversarial domain adaptation. In *Computer Vision–ECCV 2020: 16th European Conference, Glasgow, UK, August 23–28, 2020, Proceedings, Part XXIV 16*, pp. 589–606. Springer, 2020.
- Zhao, H., Des Combes, R. T., Zhang, K., and Gordon, G. On learning invariant representations for domain adaptation. In *International conference on machine learning*, pp. 7523–7532. PMLR, 2019.
- Zhu, J.-Y., Park, T., Isola, P., and Efros, A. A. Unpaired image-to-image translation using cycle-consistent adversarial networks. In *Proceedings of the IEEE international conference on computer vision*, pp. 2223–2232, 2017.
- Zhuang, Z., Zhang, Y., and Wei, Y. Gradual domain adaptation via gradient flow. In *The Twelfth International Conference on Learning Representations*, 2024.

A. Experimental Details

A.1. Implementation

For the Rotated MNIST, Color-Shift MNIST, and Portraits datasets, we implemented a CNN with three convolutional layers with 32 channels. After the encoder, we added a fully connected classifier with two hidden layers of 256 units each. For the Cover Type dataset, we adopted a similar approach using three fully connected layers with ReLU activations, where the hidden dimensions increase from 128 to 256 to 512 units, ending with an output layer matching the number of classes.

Our transport architecture includes generators composed of a single residual block containing three linear layers. The discriminator is built with three linear layers, each having 128 hidden units and paired with ReLU activation functions. We used the Adam optimizer for optimization (Kingma & Ba, 2014), Dropout for regularization (Srivastava et al., 2014), and Batch Normalization to stabilize training (Ioffe & Szegedy, 2015). The number of intermediate domains generated between source and target domains is treated as a hyperparameter, with the model’s performance evaluated for 0, 1, 2, 3, or 4 intermediate domains. All the code was ran on NVIDIA RTX 4090 GPUs.

In addition, we followed (Kumar et al., 2020) to filter out the 10% of data points where the model’s predictions exhibit the least confidence. However, instead of relying on the typical uncertainty measure, we define the confidence level as the difference between the largest and the second-largest values in the model’s output. We have found that this produces better results and we use this setting in all comparative tests.

We pretrain the encoder and classifiers f, g on four datasets, and the results of the pretrain are shown in Fig. 9, where the accuracy varies across multiple domains. All of our experiments, including ablations on the GOAT, GST method in section 5.5, are performed using the same pretrained model. With a total of six domains in the setup, the precision of the four datasets for the classifications trained on the source domain directly using the classification results in the subsequent domains are shown in Fig. 9. The accuracies fall roughly stepwise in line with our expectations for the problem setup.

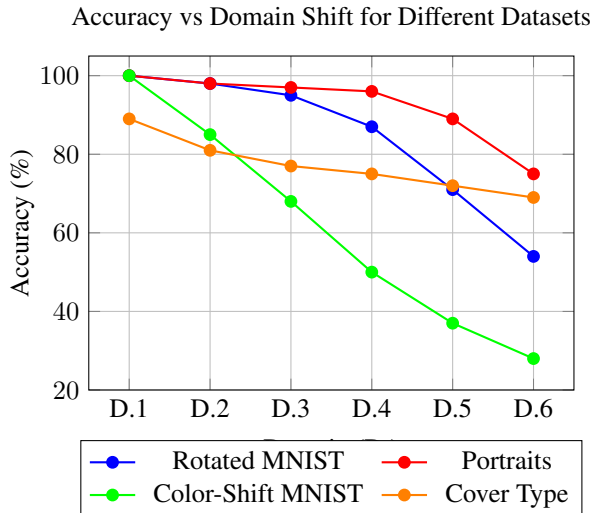


Figure 9. Accuracy of classifiers trained on Domain 1 and evaluated across progressively changing domains (D.2 to D.6) for four datasets: Rotated MNIST, Portraits, Color-Shift MNIST, and Cover Type. The figure illustrates a gradual decrease in accuracy as the domain shift increases, highlighting the impact of domain adaptation challenges.

A.2. Results of Our Method

We present a comparison of our proposed SWAT method with multiple datasets, including Rotated MNIST, Color-Shift MNIST, Portraits and Cover Type, as detailed in Tables 4 through 7. Each experiment was repeated multiple times, with the results shown as mean values along with variance intervals. The leftmost column of each table represents the performance obtained using only adversarial training, which corresponds to the method without flow matching.

In Tables 4 to 7, the column “# Given Domains” indicates the number of domains included in the experiment, comprising both the source and the target domains. The “Inter-domain counts in SWAT” columns indicate the number of inter-domain

steps taken between the given domains in the dataset. The entire process is equivalent to including (“# Given Domains - 1”) \times (“# Inter-domain counts in SWAT + 1”) + 1 training step, which includes self-training of GAN and the encoder f and classifier g . For example, with four domains and three intermediate steps, the total number of training steps is calculated as $(4 - 1) \times (3 + 1) + 1 = 13$ small steps.

Table 4. Comparison of the accuracy of our method for different given intermediate domains (including source and target domains) on the **Rotated MNIST** dataset, as well as the 68% confidence interval of the mean across 5 runs.

# Given Domains	# Inter-domain counts in SWAT				
	0	1	2	3	4
2	83.3 \pm 0.9	85.0 \pm 0.5	86.1 \pm 0.4	86.9 \pm 0.2	88.1 \pm 1.5
3	94.7 \pm 0.5	95.1 \pm 0.7	96.1 \pm 0.1	96.1 \pm 0.1	96.1 \pm 0.2
4	95.6 \pm 0.1	96.3 \pm 0.0	96.4 \pm 0.0	96.2 \pm 0.1	96.3 \pm 0.0
5	95.9 \pm 0.1	96.1 \pm 0.1	96.1 \pm 0.2	96.5 \pm 0.2	96.5 \pm 0.2
6	95.9 \pm 0.3	96.4 \pm 0.2	95.5 \pm 1.5	96.6 \pm 0.1	96.7 \pm 0.1

Table 5. Comparison of the accuracy of our method for different given intermediate domains (including source and target domains) on the **Color-Shift MNIST** dataset, as well as the 68% confidence interval of the mean across 5 runs.

# Given Domains	# Inter-domain counts in SWAT				
	0	1	2	3	4
2	96.9 \pm 0.6	96.6 \pm 1.9	94.9 \pm 5.3	98.8 \pm 0.3	98.0 \pm 1.0
3	97.9 \pm 1.9	99.4 \pm 0.1	99.4 \pm 0.0	99.2 \pm 0.4	99.5 \pm 0.0
4	99.4 \pm 0.0	99.6 \pm 0.0	99.5 \pm 0.0	99.5 \pm 0.1	99.6 \pm 0.0
5	99.5 \pm 0.0	99.6 \pm 0.0	99.5 \pm 0.1	99.4 \pm 0.3	99.5 \pm 0.1
6	99.6 \pm 0.0	99.4 \pm 0.3	99.2 \pm 0.5	99.4 \pm 0.1	99.5 \pm 0.1

Table 6. Comparison of the accuracy of our method for different given intermediate domains (including source and target domains) on the **Portraits** dataset, as well as the 68% confidence interval of the mean across 5 runs.

# Given Domains	# Inter-domain counts in SWAT				
	0	1	2	3	4
2	82.9 \pm 1.2	84.6 \pm 0.2	85.0 \pm 0.9	85.1 \pm 0.2	85.3 \pm 0.1
3	84.3 \pm 0.1	84.3 \pm 0.1	84.7 \pm 0.3	84.8 \pm 1.0	84.5 \pm 0.1
4	84.4 \pm 0.6	84.1 \pm 0.1	84.5 \pm 1.8	86.1 \pm 0.3	85.6 \pm 1.1
5	86.1 \pm 0.1	87.0 \pm 0.4	87.0 \pm 0.2	86.7 \pm 0.3	86.5 \pm 0.9
6	87.4 \pm 0.2	87.2 \pm 0.4	86.8 \pm 0.7	86.1 \pm 0.5	86.1 \pm 0.6

Table 7. Comparison of the accuracy of our method for different given intermediate domains (including source and target domains) on the **Cover Type** dataset, as well as the 68% confidence interval of the mean across 5 runs.

# Given Domains	# Inter-domain counts in SWAT				
	0	1	2	3	4
2	74.1 \pm 0.0	75.0 \pm 0.0	75.0 \pm 0.0	75.0 \pm 0.0	75.0 \pm 0.0
3	74.2 \pm 0.1	74.3 \pm 0.3	74.2 \pm 0.5	74.0 \pm 0.1	74.3 \pm 0.2
4	74.5 \pm 0.1	74.6 \pm 0.1	74.5 \pm 0.2	74.3 \pm 0.1	74.3 \pm 0.2
5	74.6 \pm 0.1	74.3 \pm 0.7	74.1 \pm 0.3	74.3 \pm 0.2	74.4 \pm 0.1
6	73.6 \pm 0.3	73.7 \pm 0.2	73.7 \pm 0.2	73.5 \pm 0.5	73.5 \pm 0.3

Our results demonstrate the effectiveness of the SWAT method across multiple datasets: Rotated MNIST, Color-Shift MNIST, Portraits, and Cover Type. In each case, we vary the number of given domains and the inter-domain steps in SWAT, comparing the model’s performance as the number of inter-domain steps increases.

In the results presented in Table 4 (Rotated MNIST), Table 5 (Color-Shift MNIST), and Table 6 (Portraits), SWAT shows a consistent improvement in accuracy as the number of inter-domain steps increases. Specifically, in Table 4, for the scenario where only the source and destination domains are provided (the first row), the accuracy begins at 83.3% with zero inter-domain steps and progressively increases, reaching 88.1% at four inter-domain steps. This steady enhancement in performance underscores the value of the additional inter-domain steps in improving SWAT’s generalization capacity.

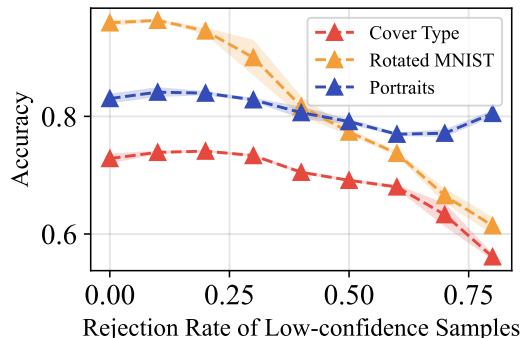


Figure 10. Accuracy vs. Rejection Rate of Low-confidence Samples for Rotated MNIST, Portrait and Cover Type Datasets. Explanation This case involves four given fields and a two-step iteration process is performed between the fields.

Furthermore, focusing on the scenario with zero inter-domain steps, the results suggest that SWAT continues to exhibit improvements across more complex datasets. This suggests that even without inter-domain steps, the model benefits from the progressive adversarial feature matching, enhancing its ability to adapt and generalize effectively across domains.

In the results presented in Table 7 (Cover Type), SWAT shows relatively stable accuracy across different numbers of inter-domain steps. Unlike other datasets like Rotated MNIST, where accuracy increases noticeably with inter-domain steps, the accuracy on the Cover Type dataset remains relatively stable. This suggests that SWAT may already be achieving near optimal performance with fewer inter-domain steps on this particular dataset. This could suggest that the model has already captured the most critical features of the dataset, or that Cover Type may be less complex compared to the other datasets, requiring fewer inter-domain steps for effective transfer learning.

It is important to highlight that the highest accuracy points are typically found in the upper-right and lower-left corners of the table. This suggests that as the number of given domains increases, the adversarial flow matching tends to become more complete, eliminating the need for additional intermediate steps to refine the flow. This observation demonstrates that our method of constructing flows matching between domains is particularly effective when only a few domains are given, and the sliding window adversarial training is highly effective all the time.

In our experiments, we observed that increasing the rejection rate of low-confidence samples, as discussed in section A.1, improves model accuracy by preventing learning from incorrect samples like Fig. 10. However, excessive rejection can harm the model’s generalization ability. This finding is intended to inspire further research in this area.